JOURNAL OF
Optical Communications
and Networking

Hybrid 3DMA for multi-user MIMO-VLC

Chen Chen,[1,*] Ruochen Zhang,[1] Wanli Wen,[1] Min Liu,[1] Pengfei Du,[2] Yanbing Yang,[3] and Xiukai Ruan[4,5]

[1]School of Microelectronics and Communication Engineering, Chongqing University, Chongqing 400044, China
[2]A*STAR's Singapore Institute of Manufacturing Technology (SIMTech), Singapore 138634, Singapore
[3]College of Computer Science, Sichuan University, Chengdu 610065, China
[4]College of Electrical and Electronic Engineering, Wenzhou University, Wenzhou 325035, China
[5]Institute of Intelligent Locks, Wenzhou University, Wenzhou 325035, China
*Corresponding author: c.chen@cqu.edu.cn

Received 23 June 2022; revised 16 August 2022; accepted 17 August 2022; published 9 September 2022

In this paper, we propose and investigate a hybrid three-dimensional multiple access (3DMA) scheme for multi-user multiple-input multiple-output visible light communication (MU-MIMO-VLC) systems that can fully exploit the 3D resources of the system including frequency, space, and power. Particularly, all users in the MU-MIMO-VLC system applying hybrid 3DMA are first divided into multiple user groups (UGs) in the spatial domain, and users within each UG are further divided into multiple user pairs (UPs) in the frequency domain. In each UP, two users are multiplexed in the power domain via superposition coding. Due to the efficient 3D resource allocation in the MU-MIMO-VLC system applying hybrid 3DMA, the available bandwidth of each user can be substantially increased. Moreover, the impact of error propagation caused by imperfect successive interference cancellation (SIC) is considered, and the optimal power allocation (OPA) strategy is also derived to maximize the achievable sum rate of each UP. The feasibility and superiority of the proposed hybrid 3DMA with OPA have been successfully verified by the obtained analysis and simulation results. It is shown that the achievable average sum rate of an indoor 4 × 4 MU-MIMO-VLC system can be substantially improved by applying the proposed hybrid 3DMA with OPA, in comparison to benchmark schemes such as orthogonal frequency division multiple access and space division multiple access. Moreover, it is further revealed that hybrid 3DMA with OPA exhibits high tolerance against imperfect SIC induced error propagation, which also shows excellent robustness and performance consistency to support multiple randomly located users.

https://doi.org/10.1364/JOCN.468749

1. INTRODUCTION

With the emergence of data-hungry applications such as ultra-high-definition video streaming, online video gaming, and virtual/augmented/extended reality (VR/AR/XR) in recent years, the global demand for high-data-rate wireless communication is increasing rapidly. It might be challenging for traditional radio frequency (RF) communication technologies to support the exponentially increased data traffic in the near future, due to the highly congested RF spectrum and the severe interference among wireless devices [1]. Lately, optical wireless communication (OWC) has been recognized as a promising technology to alleviate the RF spectrum congestion, which can utilize a hug spectrum by exploiting visible light, infrared, or ultra-violet bands [2]. Moreover, an OWC network consists of small communication cells, i.e., attocells, which can efficiently reduce device interference and enable dense spatial reuse [3]. More particularly, owing to the pervasive application of light-emitting diodes (LEDs) for general indoor illumination, visible light communication (VLC) employing illumination LEDs has been triggering tremendous interest recently [4,5]. VLC has been widely envisioned as a promising complementary technology to traditional RF technologies, which exploits the visible light spectrum ranging from 380 to 780 nm by reusing LED fixtures [6].

Although VLC systems have abundant unregulated spectrum resources, the available modulation bandwidth is largely limited by the adopted LED transmitters, especially for commercially available white LEDs [7]. To address the bandwidth limitation issue of practical VLC systems, two main categories of techniques have been reported so far: one is to extend the modulation bandwidths of LEDs through blue filtering [8], pre-equalization [9,10], or post-equalization [11,12], and the other is to increase the spectral efficiency of VLC systems for a given modulation bandwidth via advanced modulation and transmission techniques [13–15]. More specifically, multiple-input multiple-output (MIMO) transmission has been shown to be a natural and efficient way to boost the spectral efficiency of VLC systems [16]. Among all the reported MIMO techniques for VLC systems in the literature, spatial multiplexing is the most popular one, which can achieve high multiplexing

gain and hence is capable of substantially enhancing the spectral efficiency of VLC systems [17]. It should be noted that MIMO is referred to as spatial multiplexing in the following.

A. Related Work and Motivation

The investigation of MIMO transmission in VLC systems has attracted great attention recently, such as angular-diversity-based detection [18], coverage analysis [19], transceiver design [20,21], and neural-network-based joint spatial and temporal equalization [22]. So far, many experimental MIMO-VLC systems have been reported in the literature, such as a Gbit/s MIMO-VLC system using orthogonal frequency division multiplexing (OFDM) [23], a 50 Mbit/s MIMO-VLC system using on–off keying (OOK) [24], a pairwise coding-enhanced MIMO-VLC system [25], and the application of MIMO-VLC in a hospital [26,27].

Moreover, considering that there might be multiple users within the MIMO-VLC system, the design of an efficient multiple access scheme for multi-user MIMO-VLC (MU-MIMO-VLC) systems is of practical significance. Table 1 compares the main pros and cons of multiple access schemes for MU-MIMO-VLC systems.

On one hand, multiple access schemes proposed for general MU-VLC systems, such as orthogonal multiple access (OMA) schemes including time division multiple access (TDMA) [38], code division multiple access (CDMA) [39], orthogonal frequency division multiple access (OFDMA) [40] and non-OMA (NOMA) schemes [41–43], are also applicable to MU-MIMO-VLC systems. More specifically, TDMA has been adopted to support multiple users in MU-MIMO-VLC systems in [28,29], CDMA has been applied in MU-MIMO-VLC systems in [30], MU-MIMO-VLC systems using OFDMA have been studied in [31], and NOMA has been introduced in MU-MIMO-VLC systems in [32–34]. For MU-MIMO-VLC systems applying OMA schemes, MU interference (MUI) can be eliminated by allocating different users with orthogonal time/code/frequency resources, under the condition of reduced available resources of each user. For MU-MIMO-VLC systems employing NOMA schemes, the available resource of each user can be efficiently increased by multiplexing multiple users in the same resource block, but the MUI becomes nonnegligible. Nevertheless, the spatial characteristics of MIMO-VLC systems are not fully exploited when using OMA and NOMA schemes.

On the other hand, MIMO-specific multiple access schemes have also been designed for MU-MIMO-VLC systems. By performing power allocation (PA) among LEDs, precoding can be conducted to remove MUI at the transmitter side in MU-MIMO-VLC systems [21,35,36]. However, due to the limited dynamic range and severe nonlinearity of LEDs, the performance of precoding might be significantly degraded in practical MU-MIMO-VLC systems [44]. In our previous work [37], we proposed a space division multiple access (SDMA) scheme for MU-MIMO-VLC systems that exploits both the spatial domain and frequency domain resources of the system. According to the distinctive spatial positions of LEDs and the relative positions of users with respect to each LED, users within the MU-MIMO-VLC system are divided into multiple groups, and each group can use the overall modulation bandwidth of the system. Hence, the proposed SDMA scheme can utilize the modulation bandwidth more efficiently than conventional OFDMA. Nevertheless, OFDMA is still adopted to support users within each group in the MU-MIMO-VLC system applying SDMA, which inevitably leads to the reduction of available bandwidth of each user, especially when there is a large number of users within the group. Therefore, it is necessary to design a more efficient multiple access scheme for MU-MIMO-VLC systems by fully exploiting three degrees of resources in the system.

B. Main Contributions

To further enhance the bandwidth utilization efficiency of MU-MIMO-VLC systems, in this paper, we propose a hybrid three-dimensional multiple access (3DMA) scheme for MU-MIMO-VLC systems. The main contributions of this work can be summarized as follows:

- proposal of a hybrid 3DMA scheme for MU-MIMO-VLC systems that can fully exploit the 3D resources of the system including frequency, space, and power;
- analytical derivation of the achievable rate of the MU-MIMO-VLC system applying the proposed hybrid 3DMA scheme and other benchmark schemes;
- formulating an analytical optimization problem to maximize the achievable sum rate and further deriving the optimal power allocation (OPA) strategy for MU-MIMO-VLC systems applying hybrid 3DMA;

Table 1. Comparison of Multiple Access Schemes for MU-MIMO-VLC Systems

Scheme	Reference	Pros	Cons
TDMA	[28,29]	Negligible MUI	Reduced available time slots, spatial characteristics ignored
CDMA	[30]	Negligible MUI	Reduced available codes, spatial characteristics ignored
OFDMA	[31]	Negligible MUI	Reduced available bandwidth, spatial characteristics ignored
NOMA	[32–34]	Increased available bandwidth	Nonnegligible MUI, spatial characteristics ignored
Precoding	[21,35,36]	Negligible MUI, spatial characteristics exploited	Vulnerable to dynamic range limitation, vulnerable to LED nonlinearity
SDMA	[37]	Negligible MUI, spatial characteristics exploited	Reduced available bandwidth, only spatial and frequency resources exploited
Hybrid 3DMA	This work	Increased available bandwidth, three degrees of resources exploited	Nonnegligible MUI

• validating the analytical predictions through extensive Monte Carlo simulations, and presenting insightful results about the achievable rate performance of the MU-MIMO-VLC system using various multiple access schemes under the impact of imperfect successive interference cancellation (SIC) induced error propagation.

The rest of this paper is organized as follows. Section 2 introduces the general model of MU-MIMO-VLC systems. In Section 3, the principle of the proposed hybrid 3DMA is first described, the achievable rate of the MU-MIMO-VLC system using hybrid 3DMA is further analyzed, and the OPA strategy in hybrid 3DMA is also derived. Section 4 presents the detailed analytical and simulation results. Finally, Section 5 gives the conclusion of the paper.

2. GENERAL MODEL OF MU-MIMO-VLC

In this section, we introduce the basic mathematical model of a general indoor MU-MIMO-VLC system, where N LEDs are installed in the ceiling, and K users are located over the receiving plane. Each user is equipped with N photodiodes (PDs) that face towards the ceiling vertically. For simplicity and without loss of generality, we here assume that the MU-MIMO-VLC system has a flat frequency response. (A flat frequency response can be easily ensured by applying efficient frequency domain pre-equalization/post-equalization in a digital or analog manner [9,10].) Letting $\mathbf{x}=[x_1, x_2, \ldots, x_N]^T$ be the transmitted electrical signal vector with power P_s, the received signal vector at the kth user, i.e., $\mathbf{y}_k=[y_{k,1}, y_{k,2}, \ldots, y_{k,N}]^T$, can be expressed by

$$\mathbf{y}_k=\mathbf{H}_k\mathbf{x}+\mathbf{z}_k, \tag{1}$$

where $\mathbf{H}_k$ denotes the $N\times N$ channel matrix for the kth user, and $\mathbf{z}_k=[z_{k,1}, z_{k,2}, \ldots, z_{k,N}]^T$ is the corresponding additive noise vector. The channel matrix $\mathbf{H}_k$ is given by

$$\mathbf{H}_k=\begin{bmatrix} h_{k,11} & \cdots & h_{k,1N} \\ \vdots & \ddots & \vdots \\ h_{k,N1} & \cdots & h_{k,NN} \end{bmatrix}, \tag{2}$$

where $h_{k,rt}$ $(r=1, 2, \ldots, N;\ t=1, 2, \ldots, N)$ denotes the channel gain between the rth PD and the tth LED at the kth user.

In practical VLC systems, the channel gain $h_{k,rt}$ usually consists of both the line-of-sight (LOS) component $h_{k,rt,\mathrm{LOS}}$ and non-LOS (NLOS) component $h_{k,rt,\mathrm{NLOS}}$, i.e., $h_{k,rt}=h_{k,rt,\mathrm{LOS}}+h_{k,rt,\mathrm{NLOS}}$ [6]. Assuming each LED follows a Lambertian radiation pattern, the LOS channel gain $h_{k,rt,\mathrm{LOS}}$ can be calculated by

$$h_{k,rt,\mathrm{LOS}}=\frac{(m+1)\rho A}{2\pi d_0^2}\cos^m(\varphi_0)\,G_f G_l\cos(\theta_0), \tag{3}$$

where $m=-\ln 2/\ln(\cos(\Psi))$ denotes the order of Lambertian emission, and Ψ is the semi-angle at half power (SAHP) of the LED; ρ and A are the responsivity and the active area of the PD, respectively; d_0 is the distance between the rth PD in the kth user and the tth LED; φ_0 is the emission angle; θ_0 is the incident angle; and G_f and G_l are the gains of optical filter and lens, respectively. The gain of the optical lens is given by $G_l=\frac{n_{\mathrm{RI}}^2}{\sin^2\Phi}$, where n_{RI} and Φ are the refractive index (RI) and the half-angle field-of-view (FOV) of the lens, respectively.

Moreover, assuming only the first reflection is considered, the NLOS channel gain $h_{k,rt,\mathrm{NLOS}}$ can be obtained by [6,45]

$$h_{k,rt,\mathrm{NLOS}}=\int \frac{(m+1)\rho\varepsilon A}{2(\pi d_1 d_2)^2}\cos^m(\varphi)\cos(\phi_1)\cos(\phi_2) \times G_f G_l\cos(\theta)\mathrm{d}A_w, \tag{4}$$

where d_1 and d_2 denote the distance between the reflective point and the tth LED and the distance between the rth PD and the reflective point, respectively; ε is the reflectivity of the wall; φ is the emission angle from the LED, ϕ_1 is the incident angle to the reflective point, ϕ_2 is the emission angle from the reflective point, and θ is the incident angle to the PD; and dA_w is a small reflective area on the wall.

At the kth user, the transmitted electrical signal vector can be estimated via MIMO demultiplexing. Here, we adopt the zero-forcing (ZF) approach to perform MIMO demultiplexing, due to its simplicity and low complexity [13,46]. After ZF-based MIMO demultiplexing, the estimate of the transmitted electrical signal vector is obtained as follows:

$$\hat{\mathbf{x}}_k=\mathbf{H}_k^{\dagger}\mathbf{y}_k=\mathbf{x}+\mathbf{H}_k^{\dagger}\mathbf{z}_k, \tag{5}$$

where $\mathbf{H}_k^{\dagger}$ denotes the pseudo inverse of $\mathbf{H}_k$, which is given by $\mathbf{H}_k^{\dagger}=(\mathbf{H}_k^{*}\mathbf{H}_k)^{-1}\mathbf{H}_k^{*}$, with $\mathbf{H}_k^{*}$ being the conjugated transpose of $\mathbf{H}_k$ and $(\cdot)^{-1}$ being the inverse of a matrix [16]. Letting $\tilde{h}_{k,rt}$ denote the element in the tth row and the rth column of $\mathbf{H}_k^{\dagger}$, the estimate of the tth data stream corresponding to the tth LED at the kth user is expressed by

$$\hat{x}_{k,t}=x_t+\sum_{r=1}^{N}\tilde{h}_{k,rt}z_{k,r}. \tag{6}$$

Moreover, the additive noise can be reasonably modeled as a real-valued zero-mean additive white Gaussian noise (AWGN), which consists of both thermal and shot noises. The power of the AWGN is calculated by $P_z=N_0 B$, where N_0 denotes the power spectral density (PSD), and B is the modulation bandwidth [17].

3. MU-MIMO-VLC USING HYBRID 3DMA

In this section, we describe the detailed principle of the MU-MIMO-VLC system using hybrid 3DMA. Figure 1 illustrates the resource allocation strategies in a K-user $N\times N$ MU-MIMO-VLC system using different multiple access techniques. When employing FDMA/OFDMA, as shown in Fig. 1(a), the overall bandwidth B is partitioned and shared by all K users, and therefore the available bandwidth of each user becomes very small [40]. Assuming equal bandwidth allocation among users, the available bandwidth of the kth user is given by $B_k=\frac{B}{K}$. When applying SDMA, as shown in Fig. 1(b), the K users are first divided into multiple user groups (UGs) based on their spatial locations with respect to the LED transmitters. As a result, each UG can utilize the overall system bandwidth

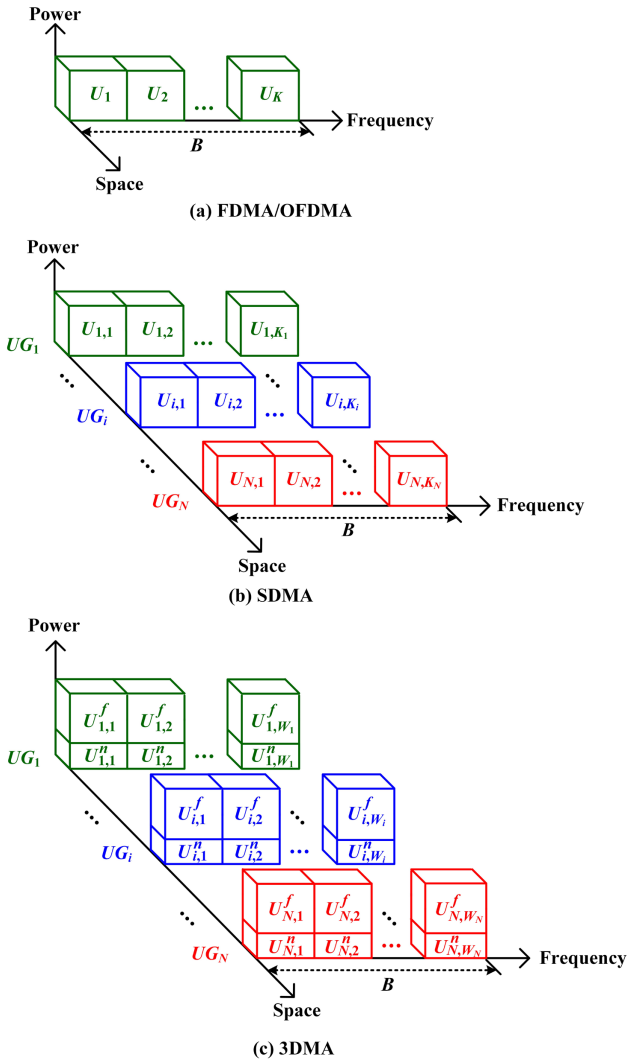

Fig. 1. Illustration of resource allocation in a K-user $N \times N$ MU-MIMO-VLC system using (a) FDMA/OFDMA, (b) SDMA, and (c) hybrid 3DMA.

B, which is further partitioned and shared by users within each UG [37]. Assuming the ith ($i = 1, 2, \ldots, N$) UG, i.e., UG_i, consists of K_i users and equal bandwidth allocation among users within each UG, the available bandwidth of the kth user in UG_i is given by $B_{k,i} = \frac{B}{K_i}$. When using the proposed hybrid 3DMA, as shown in Fig. 1(c), users within each UG are further paired together. (For the UG with an odd number of users, the remaining unpaired user can be allocated with separate power and bandwidth resources [42].) Specifically, the overall system bandwidth B is partitioned and shared by all user pairs (UPs) in each UG and power domain NOMA is applied for two users within each UP. (It is practical to multiplex only two users in the power domain considering the decoding computational complexity and time delay at the receiver side [47].) Assuming there are W_i UPs in UG_i and equal bandwidth allocation among UPs within each UG, the available bandwidth of the kth user in $\mathrm{UP}_{i,j}$ ($j = 1, 2, \ldots, W_i$) is given by $B_{k,ij} = \frac{B}{W_i}$. It can be seen from Fig. 1 that FDMA/OFDMA utilizes only frequency domain resources to support multiple users, while SDMA uses both space and frequency domain resources to serve multiple users. For the proposed hybrid 3DMA, 3D resources, including space, frequency, and power, are adopted to realize multiple access in MU-MIMO-VLC systems.

A. Principle of Hybrid 3DMA

Figure 2 illustrates the schematic diagram of a K-user $N \times N$ MU-MIMO-VLC system using hybrid 3DMA. As we can see, the input data of each user are first mapped into quadrature amplitude modulation (QAM) symbols, and then 3D resource allocation is performed. After parallel OFDM encoding, the resultant signals are used to drive N LEDs. At the receiver side, each user detects the optical signal via N PDs. Subsequently, MIMO demultiplexing and parallel OFDM decoding are conducted. After that, pairwise 3D signal recovery is performed with respect to each UP, and the recovered QAM symbols are finally demapped to generate the users' output data. The detailed procedures to execute 3D resource allocation and pairwise 3D signal recovery are described as follows.

1. 3D Resource Allocation

Figure 2(a) shows the procedures to implement 3D resource allocation in the K-user $N \times N$ MU-MIMO-VLC system using hybrid 3DMA. First, K users are divided into N UGs via space channel allocation in the space domain, which can be performed according to the obtained channel gains. Specifically, the sum channel gain of the kth user with respect to the tth LED can be defined as $h_{k,t} = \sum_{r=1}^{N} h_{k,rt}$, and the corresponding sum channel gain vector with respect to all the N LEDs can be obtained by

$$\mathbf{h}_k = \left[h_{k,1}, h_{k,2}, \ldots, h_{k,N}\right]. \tag{7}$$

Based on Eq. (7), we can identify the index of the UG that the kth user belongs to, i.e., τ_k, by obtaining the index of the largest element of $\mathbf{h}_k$, which is with respect to the specific LED with which the kth user can achieve the maximum sum channel gain:

$$\tau_k = \underset{t}{\operatorname{argmax}}\, h_{k,t}, \quad t \in \{1, 2, \ldots, N\}. \tag{8}$$

Hence, the kth user is allocated with the τ_kth space channel and belongs to the τ_kth UG, which indicates that the kth user utilizes only the τ_kth PD to receive the intended signal from the τ_kth LED. Similarly, space channel allocation can be executed for all K users, which are grouped into N UGs. Considering that users might be randomly distributed over the receiving plane, some of the UGs might be empty. In this case, the LEDs corresponding to empty UGs are used only for illumination [37]. Assuming that there are totally T ($0 \le T \le N$) LEDs used for both illumination and signal transmission, the dimension of the channel matrix becomes $N \times T$, and the resultant channel matrix $\mathbf{V}_k$ can be represented as follows:

$$\mathbf{V}_k = \left[\mathbf{v}_{k,1}, \mathbf{v}_{k,2}, \ldots, \mathbf{v}_{k,T}\right]. \tag{9}$$

In Eq. (9), the vector element $\mathbf{v}_{k,q} = [v_{k,1q}, v_{k,2q}, \ldots, v_{k,Nq}]^T$ is with respect to the qth ($q = 1, 2, \ldots, T$) LED, which is activated for both illumination and signal transmission.

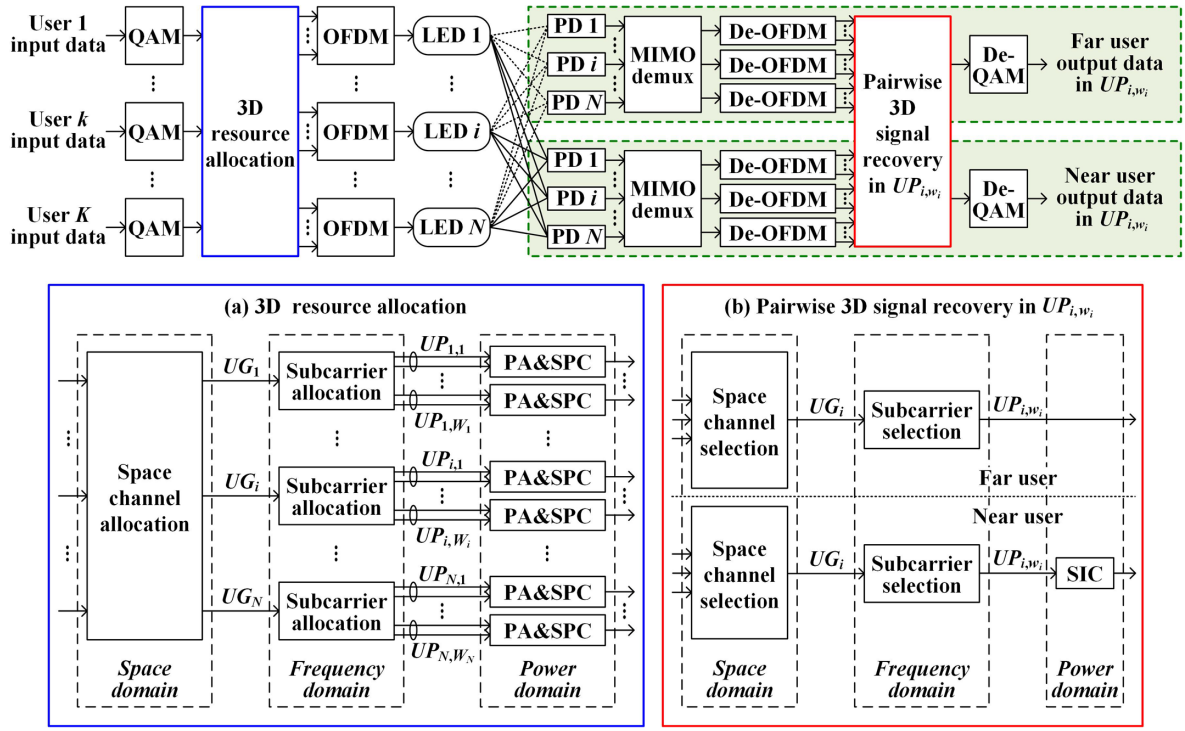

Fig. 2. Schematic diagram of a K-user $N \times N$ MU-MIMO-VLC system using hybrid 3DMA. Insets: (a) 3D resource allocation and (b) pairwise 3D signal recovery. PA, power allocation; SPC, superposition coding; SIC, successive interference cancellation.

After space channel allocation in the space domain, subcarrier allocation in the frequency domain is further carried out. As shown in Fig. 1, users within each UG are first divided into multiple UPs, and then subcarrier allocation is performed among all UPs within each UG. To perform user pairing, users within each UG are sorted based on their channel gains. Letting $h_{k_i,ii}$ $(k_i = 1, 2, \ldots, K_i)$ denote the channel gain of the k_ith user of the ith UG, the K_i users within the ith UG can be sorted in the ascending order:

$$h_{1,ii} \le \cdots \le h_{k_i,ii} \le \cdots \le h_{K_i,ii}. \tag{10}$$

According to the above user sorting, channel-based user pairing can be performed as follows. For the case in which the ith UG consists of an even number of users, i.e., $K_i = 2W_i$, the sorted K_i users are first divided into two groups. Specifically, the first group g_{i1}^e contains the first half of the sorted users starting from user 1 to user $\frac{K_i}{2}$, while the second group g_{i2}^e contains the second half starting from user $\frac{K_i}{2}+1$ to user K_i. Subsequently, user pairing can be conducted in the following manner: $\mathrm{UP}_{i,w_i}^e = [g_{i1}^e(w_i), g_{i2}^e(w_i)]$, i.e., the w_ith user pair UP_{i,w_i}^e contains both the w_ith user in g_{i1}^e and the w_ith user in g_{i2}^e with $w_i = 1, 2, \ldots, W_i$. For the case in which the ith UG consists of an odd number of users, i.e., $K_i = 2W_i - 1$, the sorted K_i users are divided into three groups. To be more specific, the first group g_{i1}^o contains $\frac{K_i-1}{2}$ users starting from user 1 to user $\frac{K_i-1}{2}$, the second group g_{i2}^o also contains $\frac{K_i-1}{2}$ users starting from user $\frac{K_i+3}{2}$ to user K_i, and the third group g_{i3}^o contains only one user, i.e., user $\frac{K_i+1}{2}$. After that, user pairing can be performed as follows. For UP_{i,w_i}^o with $w_i = 1, 2, \ldots, W_i - 1$, it is obtained by $\mathrm{UP}_{i,w_i}^o = [g_{i1}^o(w_i), g_{i2}^o(w_i)]$, i.e., the w_ith user pair UP_{i,w_i}^o contains both the w_ith user in g_{i1}^o and the w_ith user in g_{i2}^o. For UP_{i,W_i}^o, it contains only user $\frac{K_i+1}{2}$, which can utilize all the bandwidth and power sources allocated to the UP. As a result, user pairing can be successfully implemented based on their channel gains.

Given the obtained multiple UPs, power domain NOMA is adopted to support the two users within each UP. For each UP, as shown in Fig. 2(a), PA is first performed between two users and then power domain superposition coding (SPC) is further executed. In the w_ith UP of the ith UG, i.e., UP_{i,w_i}, the two users are sorted as a far user U_{i,w_i}^f and a near user U_{i,w_i}^n according to their channel gains. Letting p_{i,w_i}^f and p_{i,w_i}^n respectively denote the electrical transmit powers allocated to the far user and near user, the PA ratio between the near user and far user in UP_{i,w_i} can be defined as follows:

$$\alpha_{w_i} = \frac{p_{w_i}^n}{p_{w_i}^f}, \quad 0 \le \alpha_{w_i} \le 1. \tag{11}$$

Assuming that the total electrical transmit power of each UP is a constant value P_s, we have $P_s = p_{w_i}^f + p_{w_i}^n$. As a result, the electrical transmit powers of far and near users can be obtained by

$$\begin{cases} p_{w_i}^f = \frac{1}{1+\alpha_{w_i}} P_s, \\ p_{w_i}^n = \frac{\alpha_{w_i}}{1+\alpha_{w_i}} P_s. \end{cases} \tag{12}$$

To efficiently perform PA between the far and near users in each UP, two low-complexity channel-based PA strategies

are considered, including gain ratio PA (GRPA) [41] and normalized gain difference PA (NGDPA) [33]. Hence, the corresponding PA ratio α_{i,w_i} can be expressed by

$$\alpha_{w_i} = \begin{cases} \left(\frac{h^f_{w_i}}{h^n_{w_i}}\right)^2, & \text{GRPA} \\ \frac{h^n_{w_i} - h^f_{w_i}}{h^n_{w_i}}, & \text{NGDPA} \end{cases}, \tag{13}$$

where $h^f_{w_i}$ and $h^n_{w_i}$ denote the channel gains of far and near users in UP_{i,w_i}, respectively. Besides GRPA and NGDPA, we further consider the OPA strategy in 3D resource allocation, which is able to maximize the achievable sum rate of each UP. The detailed description of OPA will be discussed in Subsection 3.C.

Finally, SPC is performed to generate the superposed signal of each UP. Letting $s^f_{w_i}$ and $s^n_{w_i}$ respectively denote the normalized message signals intended for far and near users in UP_{i,w_i}, the resultant superposed signal is expressed by

$$s_{w_i} = \sqrt{p^f_{w_i}} s^f_{w_i} + \sqrt{p^n_{w_i}} s^n_{w_i}. \tag{14}$$

2. Pairwise 3D Signal Recovery

The procedures to carry out pairwise 3D signal recovery in each UP are depicted in Fig. 2(b). It can be seen that space channel selection is first executed in the space domain to select the allocated space channel for the ith UG, i.e., UG_i with $i = 1, 2, \ldots, N$. Subsequently, subcarrier selection is further performed in the frequency domain to select the allocated subcarriers for the w_ith UP in UG_i, i.e., UP_{i,w_i} with $w_i = 1, 2, \ldots, W_i$. For the far user in UP_{i,w_i}, the superposed signal carried by the corresponding subcarriers is directly demapped to obtain the output data. However, for the near user in UP_{i,w_i}, SIC is first conducted to estimate the signal from the superposed signal and the resultant signal is then demapped to generate the output data.

B. Achievable Rate

Based on the principle of hybrid 3DMA, we mathematically derive the achievable rate of the K-user $N \times N$ MU-MIMO-VLC system using hybrid 3DMA. (In this current work, we focus mainly on the achievable rate performance of the MU-MIMO-VLC system applying different multiple access schemes. The user fairness is another very important performance metric of MU-MIMO-VLC systems, which is out of the scope of this work and will certainly be investigated in our future work.) Considering the fact that the received signal-to-noise ratios (SNRs) of different space channels might be different due to their distinctive transmission paths, it might be difficult to utilize received SNR as the merit to evaluate the achievable rate of MU-MIMO-VLC systems [17]. Instead, we adopt transmitted SNR as the common metric for achievable rate evaluation. More specifically, the transmitted SNR γ_{tx} is defined as the ratio between the electrical power P_s of the transmitted OFDM signal at the input of each LED to the electrical power P_z of the additive noise at the receiver side, i.e., $\gamma_{tx} = \frac{P_s}{P_z}$ [16]. For the purpose of comparison, the achievable rates of MU-MIMO-VLC systems using OFDMA and SDMA are also discussed.

1. OFDMA

For conventional OFDMA-based MU-MIMO-VLC systems, each user utilizes all the space channels to transmit the intended message signals, and therefore the achievable rate of each user is the sum of the achievable rates of all space channels. According to Eq. (6), the received SNR $\gamma_{k,t}$ of the tth space channel at the kth user is obtained by

$$\gamma_{k,t} = \frac{P_s}{\sum_{r=1}^{N} \tilde{h}^2_{k,rt} P_z} = \frac{\gamma_{tx}}{\sum_{r=1}^{N} \tilde{h}^2_{k,rt}}. \tag{15}$$

Moreover, under the assumption of equal bandwidth allocation, the available bandwidth of each user in the K-user $N \times N$ MU-MIMO-VLC system is given by $\frac{B}{K}$. As a result, the achievable sum rate of the K-user $N \times N$ MU-MIMO-VLC system using OFDMA is given by [16]

$$R_{\text{OFDMA}} = \frac{B}{2K} \sum_{k=1}^{K} \sum_{t=1}^{N} \log_2 \left(1 + \frac{e\gamma_{tx}}{2\pi \sum_{r=1}^{N} \tilde{h}^2_{k,rt}}\right). \tag{16}$$

2. SDMA

For the K-user $N \times N$ MU-MIMO-VLC system using SDMA, each user employs only the single allocated space channel to transmit the intended message signal. Due to the random distribution of users, only T ($0 \le T \le N$) out of N space channels might be utilized for signal transmission, which indicates that there are totally T UGs in the system. Hence, the channel matrix becomes $\mathbf{V}_k$ with a dimension of $N \times T$, as given by Eq. (9). In consequence, the transmitted signal vector becomes $\mathbf{x}' = [x'_1, x'_2, \ldots, x'_T]^T$, and the resultant received signal vector $\mathbf{y}'_k$ at the kth user is expressed by

$$\mathbf{y}'_k = \mathbf{V}_k \mathbf{x}' + \mathbf{z}_k. \tag{17}$$

Letting $\mathbf{V}^\dagger_k$ denote the pseudo inverse of $\mathbf{V}_k$, the estimate of $\mathbf{x}'$ at the kth user after MIMO demultiplexing is given by

$$\hat{\mathbf{x}}'_k = \mathbf{V}^\dagger_k \mathbf{y}'_k = \mathbf{x}' + \mathbf{V}^\dagger_k \mathbf{z}_k, \tag{18}$$

and the estimate of the τ_kth data stream corresponding to the τ_kth space channel allocated to the kth user is described by

$$\hat{x}'_{k,\tau_k} = x'_{\tau_k} + \sum_{r=1}^{N} \tilde{v}_{k,r\tau_k} z_{k,r}, \tag{19}$$

where $\tilde{v}_{k,r\tau_k}$ denotes the element in the τ_kth row and the rth column of $\mathbf{V}^\dagger_k$. Based on Eq. (19), the received SNR γ'_{k,τ_k} of the τ_kth space channel at the kth user is obtained by

$$\gamma'_{k,\tau_k} = \frac{P_s}{\sum_{r=1}^{N} \tilde{v}^2_{k,r\tau_k} P_z} = \frac{\gamma_{tx}}{\sum_{r=1}^{N} \tilde{v}^2_{k,r\tau_k}}. \tag{20}$$

In addition, each UG in the SDMA-based MU-MIMO-VLC system can use all the system bandwidth B. For the τ_kth

UG with K_{τ_k} users, the achievable bandwidth of each user in the τ_kth UG with equal bandwidth allocation is given by $\frac{B}{K_{\tau_k}}$. Therefore, the achievable sum rate of the K-user $N \times N$ MU-MIMO-VLC system using SDMA is given by [37]

$$R_{\mathrm{SDMA}} = \frac{B}{2}\sum_{k=1}^{K}\frac{1}{K_{\tau_k}}\log_2\left(1+\frac{e\gamma_{tx}}{2\pi\sum_{r=1}^{N}\tilde{v}_{k,r\tau_k}^2}\right). \tag{21}$$

3. Hybrid 3DMA

When applying hybrid 3DMA in the K-user $N \times N$ MU-MIMO-VLC system, the users within each UG are first divided into multiple UPs according to the user pairing approach as given by Eq. (10), and power domain NOMA is further adopted to support the two users within each UP. For the w_i-UP in UG$_i$, i.e., UP$_{i,w_i}$ with $w_i = 1, 2, \ldots, W_i$ and $i = 1, 2, \ldots, T$, letting $\mathbf{s} = [s_1, s_2, \ldots, s_T]^T$ denote the transmitted signal vector, the received signal vectors at far and near users in UP$_{i,w_i}$ can be expressed by

$$\begin{cases} \mathbf{y}_{w_i}^f = \mathbf{V}_{w_i}^f\mathbf{s} + \mathbf{z}_{w_i}^f, \\ \mathbf{y}_{w_i}^n = \mathbf{V}_{w_i}^n\mathbf{s} + \mathbf{z}_{w_i}^n, \end{cases} \tag{22}$$

where $\mathbf{V}_{w_i}^f$ and $\mathbf{V}_{w_i}^n$ are the corresponding $N \times T$ channel matrices, while $\mathbf{z}_{w_i}^f$ and $\mathbf{z}_{w_i}^n$ are the corresponding noise vectors. Letting $\mathbf{V}_{w_i}^{f,\dagger}$ and $\mathbf{V}_{w_i}^{n,\dagger}$ respectively denote the pseudo inverses of $\mathbf{V}_{w_i}^f$ and $\mathbf{V}_{w_i}^n$, the estimates of $\mathbf{s}$ at far and near users in UP$_{i,w_i}$ are obtained by

$$\begin{cases} \hat{\mathbf{s}}_{w_i}^f = \mathbf{V}_{w_i}^{f,\dagger}\mathbf{y}_{w_i}^f = \mathbf{s} + \mathbf{V}_{w_i}^{f,\dagger}\mathbf{z}_{w_i}^f, \\ \hat{\mathbf{s}}_{w_i}^n = \mathbf{V}_{w_i}^{n,\dagger}\mathbf{y}_{w_i}^n = \mathbf{s} + \mathbf{V}_{w_i}^{n,\dagger}\mathbf{z}_{w_i}^n. \end{cases} \tag{23}$$

Using Eq. (14), the estimate of the intended data streams via their allocated space channels, i.e., the τ_fth and τ_nth space channels, for far and near users in UP$_{i,w_i}$ are respectively given by

$$\begin{cases} \hat{s}_{w_i}^f = \sqrt{p_{w_i}^f}s_{w_i}^f + \sqrt{p_{w_i}^n}s_{w_i}^n + \sum_{r=1}^{N}\tilde{v}_{w_i,r\tau_f}^f z_{w_i,r}^f, \\ \hat{s}_{w_i}^n = \sqrt{p_{w_i}^f}s_{w_i}^f + \sqrt{p_{w_i}^n}s_{w_i}^n + \sum_{r=1}^{N}\tilde{v}_{w_i,r\tau_n}^n z_{w_i,r}^n, \end{cases} \tag{24}$$

where $\tilde{v}_{w_i,r\tau_f}^f$ ($\tilde{v}_{w_i,r\tau_n}^n$) denotes the element in the τ_fth (τ_nth) row and the rth column of $\mathbf{V}_{w_i}^{f,\dagger}$ ($\mathbf{V}_{w_i}^{n,\dagger}$).

For the far user in UP$_{i,w_i}$, the estimated signal is directly demapped to recover the transmitted data. As a result, the received SNR of the far user in UP$_{i,w_i}$ is calculated by

$$\begin{aligned} \gamma_{w_i,\tau_f}^f &= \frac{p_{w_i}^f}{p_{w_i}^n + \sum_{r=1}^{N}\left(\tilde{v}_{w_i,r\tau_f}^f\right)^2 P_z} \\ &= \frac{P_s}{\alpha_{w_i}P_s + (1+\alpha_{w_i})\sum_{r=1}^{N}\left(\tilde{v}_{w_i,r\tau_f}^f\right)^2 P_z} \\ &= \frac{\gamma_{tx}}{\alpha_{w_i}\gamma_{tx} + (1+\alpha_{w_i})\sum_{r=1}^{N}\left(\tilde{v}_{w_i,r\tau_f}^f\right)^2}. \end{aligned} \tag{25}$$

Moreover, for the near user in UP$_{i,w_i}$, SIC is first executed with respect to the estimated signal, and the resultant signal is then demapped for data recovery, considering the fact that the SIC process might not be perfect and there might be some residual interference leading to error propagation [48,49]. Letting β $(0 \le \beta \le 1)$ denote the error propagation ratio caused by imperfect SIC, the received SNR of the near user in UP$_{i,w_i}$ can be obtained by

$$\begin{aligned} \gamma_{w_i,\tau_n}^n &= \frac{p_{w_i}^n}{\beta p_{w_i}^f + \sum_{r=1}^{N}\left(\tilde{v}_{w_i,r\tau_n}^n\right)^2 P_z} \\ &= \frac{\alpha_{w_i}P_s}{\beta P_s + (1+\alpha_{w_i})\sum_{r=1}^{N}\left(\tilde{v}_{w_i,r\tau_n}^n\right)^2 P_z} \\ &= \frac{\alpha_{w_i}\gamma_{tx}}{\beta\gamma_{tx} + (1+\alpha_{w_i})\sum_{r=1}^{N}\left(\tilde{v}_{w_i,r\tau_n}^n\right)^2}. \end{aligned} \tag{26}$$

Due to the use of SPC for two users within each UP, both users can utilize all the bandwidth allocated to the UP. For the i-UG consisting of W_i UPs, the available bandwidth of UP$_{i,w_i}$ under equal bandwidth allocation is given by $B_{w_i} = \frac{B}{W_i}$. As a result, the achievable rates of far and near users in UP$_{i,w_i}$ can be expressed by

$$\begin{cases} R_{w_i}^f = \frac{B}{2W_i}\log_2\left(1+\frac{e}{2\pi}\gamma_{w_i,\tau_f}^f\right), \\ R_{w_i}^n = \frac{B}{2W_i}\log_2\left(1+\frac{e}{2\pi}\gamma_{w_i,\tau_n}^n\right), \end{cases} \tag{27}$$

and hence, the achievable sum rate of far and near users in UP$_{i,w_i}$ can be given by

$$\begin{aligned} R_{w_i} &= R_{w_i}^f + R_{w_i}^n \\ &= \frac{B}{2W_i}\left(\log_2\left(1+\frac{e}{2\pi}\gamma_{w_i,\tau_f}^f\right) + \log_2\left(1+\frac{e}{2\pi}\gamma_{w_i,\tau_n}^n\right)\right). \end{aligned} \tag{28}$$

Finally, the achievable sum rate of the MU-MIMO-VLC system with T UGs can be achieved by

$$R_{\mathrm{3DMA}} = \sum_{i=1}^{T}\sum_{w_i=1}^{W_i}R_{w_i}. \tag{29}$$

C. Optimal Power Allocation in Hybrid 3DMA

In this subsection, we derive the OPA strategy for each UP in the MU-MIMO-VLC system using hybrid 3DMA. By substituting Eqs. (25) and (26) into Eq. (28), the achievable sum rate of the two users in UP$_{i,w_i}$ is given by

$$\begin{aligned} R_{w_i} = \frac{B}{2W_i}\Bigg(&\log_2\left(1+\frac{e}{2\pi}\frac{\gamma_{tx}}{\alpha_{w_i}\gamma_{tx} + (1+\alpha_{w_i})\sum_{r=1}^{N}\left(\tilde{v}_{w_i,r\tau_f}^f\right)^2}\right) \\ &+ \log_2\left(1+\frac{e}{2\pi}\frac{\alpha_{w_i}\gamma_{\mathrm{tx}}}{\beta\gamma_{tx} + (1+\alpha_{w_i})\sum_{r=1}^{N}\left(\tilde{v}_{w_i,r\tau_n}^n\right)^2}\right)\Bigg). \end{aligned} \tag{30}$$

By denoting $C_1 = \frac{e\gamma_{tx}}{2\pi}$, $C_2 = \gamma_{tx} + \sum_{r=1}^{N} (\tilde{v}^n_{w_i,r\tau_n})^2$, $C_3 = \sum_{r=1}^{N} (\tilde{v}^n_{w_i,r\tau_n})^2$, and $C_4 = \beta\gamma_{tx} + \sum_{r=1}^{N} (\tilde{v}^n_{w_i,r\tau_n})^2$, we can rewrite Eq. (30) as

$$R_{w_i} = \frac{B}{2W_i}\left(\log_2\left(C_2\alpha_{w_i} + C_5\right) + \log_2\left(C_5\alpha_{w_i} + C_4\right)\right) - \frac{B}{2W_i}\left(\log_2\left(C_2\alpha_{w_i} + C_3\right) + \log_2\left(C_3\alpha_{w_i} + C_4\right)\right), \tag{31}$$

where $C_5 = C_1 + C_3$.

For given C_1, C_2, C_3, and C_4, the OPA strategy $\alpha^{\mathrm{OPA}}_{w_i}$ for UP_{i,w_i} in the MU-MIMO-VLC system using hybrid 3DMA can be obtained by individually maximizing the achievable sum rate of the two users in UP_{i,w_i}. Therefore, the achievable sum rate maximization problem with respect to UP_{i,w_i} can be formulated as follows:

$$\alpha^{\mathrm{OPA}}_{w_i} = \underset{\alpha_{w_i}}{\operatorname{argmax}}\ R_{w_i} \quad \text{s.t. } 0 \le \alpha_{w_i} \le 1. \tag{32}$$

By observing Eqs. (31) and (32), we can find that the above maximization problem is a typical difference of convex (DC) programming problem, which can be efficiently solved by the convex–concave procedure (CCP) [50]. Therefore, the OPA strategy $\alpha^{\mathrm{OPA}}_{w_i}$ for UP_{i,w_i} can be easily obtained for the MU-MIMO-VLC system using hybrid 3DMA.

4. RESULTS AND DISCUSSION

In this section, we conduct Monte Carlo simulations to substantiate the derived analytical results in terms of achievable rates of the MU-MIMO-VLC systems applying OFDMA, SDMA, and the proposed hybrid 3DMA scheme. Without loss of generality, we consider a 4×4 (i.e., $N = 4$) MIMO-VLC system within a typical 4 m × 4 m × 3 m room. The geometry setup of the 4×4 MIMO-VLC system is depicted in Fig. 3(a), where the square 2×2 LED array is mounted at the center of the ceiling and oriented downwards to point straight to the receiving plane; the receiving plane is 0.85 m above the floor, and the square 2×2 PD array of each user located over the receiving plane is vertically oriented towards the ceiling. The spacing between two adjacent LEDs in the LED array is 2 m, while PD spacing is 10 cm. Moreover, to achieve relatively high SNRs at the receiver side, high-sensitivity avalanche PDs (APDs) are used in the PD array, which have a responsivity of 15 A/W with an active area of 19.6 mm^2 [51]. If not otherwise specified, the simulation parameters of the considered indoor MU-MIMO-VLC system are listed in Table 2. To perform SNR estimation for achievable rate calculation, binary phase-shift keying (BPSK)-based OFDM signals are transmitted by each LED, and the SNR value of each received OFDM signal is estimated from the error vector magnitude (EVM) of the corresponding BPSK constellation [37]. Moreover, since multiple users are assumed to be randomly located within the receiving plane at each simulation, we repeat the simulations 10,000 times for each case so as to obtain a stable average sum rate for fair and accurate performance evaluation.

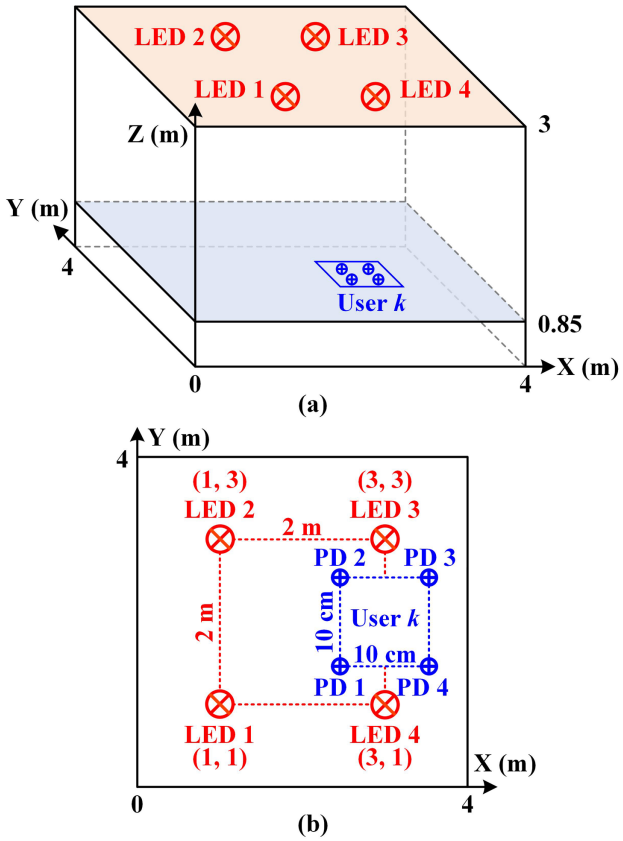

Fig. 3. (a) Geometry setup and (b) top view of the 4×4 MIMO-VLC system.

Table 2. Simulation Parameters

Parameter	Value	Reference
Room dimension	4 m × 4 m × 3 m	[46]
Height of receiving plane	0.85 m	[46]
Number of LEDs	4	[46]
LED spacing	2 m	[46]
SAHP of LED	65°	[46]
Gain of filter	0.9	[46]
RI of lens	1.5	[46]
Half-angle FOV of lens	65°	[46]
Number of APDs	4	[46]
APD spacing	10 cm	[46]
Responsivity of APD	15 A/W	[51]
Active area of APD	19.6 mm^2	[51]
Reflectivity of wall	0.8	[45]
Modulation bandwidth	20 MHz	[46]
Noise PSD	$10^{-22}\mathrm{A}^2/\mathrm{Hz}$	[17]

We first investigate the relationship between the average sum rate and the transmitted SNR for the 4×4 MIMO-VLC system applying different multiple access schemes, where the number of users is set to 15. Figures 4(a), 4(b), and 4(c) show the average sum rates versus the transmitted SNR for OFDMA, SDMA, and hybrid 3DMA with error propagation ratios of $\beta = 0$, 0.05, and 0.1, respectively. For the case of perfect SIC without error propagation, i.e., $\beta = 0$, as shown in Fig. 4(a), OFDMA always has the lowest average sum rate

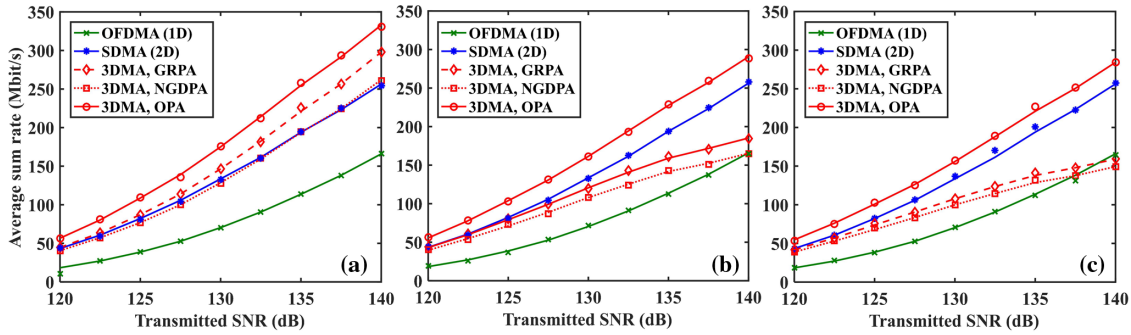

Fig. 4. Average sum rate versus transmitted SNR for OFDMA, SDMA, and hybrid 3DMA with error propagation ratios of (a) $\beta = 0$, (b) $\beta = 0.05$, and (c) $\beta = 0.1$. Lines and markers show the analysis and simulation results, respectively.

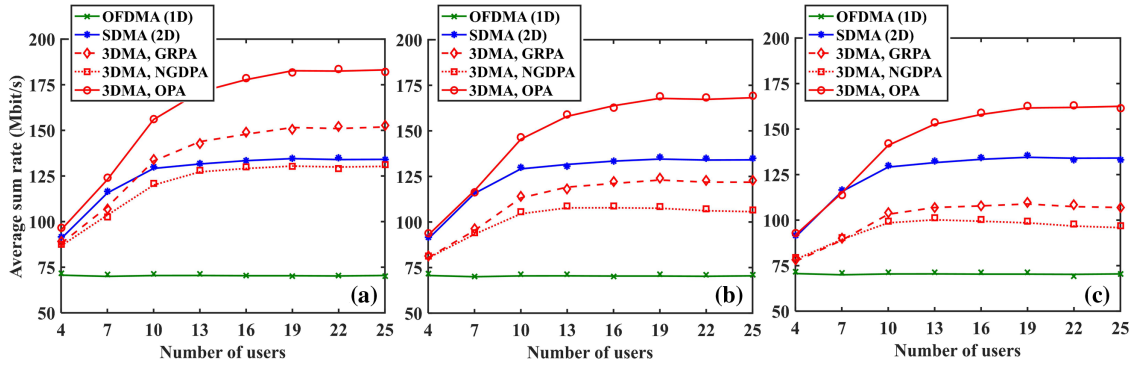

Fig. 5. Average sum rate versus number of users for OFDMA, SDMA, and hybrid 3DMA with error propagation ratios of (a) $\beta = 0$, (b) $\beta = 0.05$, and (c) $\beta = 0.1$. Lines and markers show the analysis and simulation results, respectively.

within the transmitted SNR range from 120 to 140 dB. In contrast, SDMA greatly outperforms OFDMA, and the average sum rate improvement becomes much more significant when a higher transmitted SNR is considered, which is due mainly to the enhanced bandwidth utilization efficiency of SDMA in comparison to OFDMA. Furthermore, the proposed hybrid 3DMA with OPA always achieves the highest average sum rate, and hybrid 3DMA with NGDPA obtains nearly the same average sum rate as SDMA. More specifically, the average sum rates of hybrid 3DMA with OPA, SDMA, and OFDMA at a transmitted SNR of 130 dB are 176.1, 132.6, and 70.4 Mbit/s, respectively. As a result, an average sum rate improvement of 32.8% can be obtained by the proposed hybrid 3DMA with OPA when compared with SDMA. For the case of imperfect SIC, as can be seen from Figs. 4(b) and 4(c), the average sum rates of hybrid 3DMA schemes are gradually reduced with the increase of the error propagation ratio. For a moderate error propagation ratio of $\beta = 0.05$, the average sum rates of hybrid 3DMA with GRPA and NGDPA become lower than that of SDMA, especially when the transmitted SNR is relatively large. For a severe error propagation ratio of $\beta = 0.1$, the average sum rates of hybrid 3DMA with GRPA and NGDPA can be lower than that of OFDMA when the transmitted SNR reaches 140 dB. However, hybrid 3DMA with OPA can always achieve the highest average sum rate within the entire SNR region for both moderate and severe error propagation levels. Moreover, it can be clearly observed from Fig. 4 that the simulation results agree well with the analytical predictions for all cases.

Next, we evaluate the relationship between the average sum rate and the number of users for the 4×4 MIMO-VLC system applying different multiple access schemes, where the transmitted SNR is set to 130 dB. Figures 5(a), 5(b), and 5(c) show the average sum rates versus the number of users for OFDMA, SDMA, and hybrid 3DMA with error propagation ratios of $\beta = 0$, 0.05, and 0.1, respectively. As we can see, the average sum rate of OFDMA is stable and is not affected by the number of users. In contrast, the average sum rates of SDMA and hybrid 3DMA first gradually increase when the number of users is increased from 4 to 16, which then become stable when there are more than 16 users randomly located within the receiving plane of the system. For the case of perfect SIC, i.e., $\beta = 0$, as shown in Fig. 5(a), the average sum rates of OFDMA and SDMA are 70.3 and 133.4 Mbit/s, respectively, when the number of users is 16. Moreover, the proposed hybrid 3DMA with NGDPA performs slightly worse than SDMA, while hybrid 3DMA with OPA achieves the highest average sum rate of 178.7 Mbit/s when the number of users is 16. Hence, a stable average sum rate improvement of 34% is obtained by hybrid 3DMA with OPA in comparison to SDMA when the number of users is more than 16. For the case of imperfect SIC with $\beta = 0.05$ and 0.1, as shown in Figs. 5(b) and 5(c), SDMA can outperform hybrid 3DMA with both GRPA and NGDPA. Nevertheless, the highest average sum rate is always achieved by hybrid 3DMA with OPA for both moderate and severe error propagation levels. In addition, we can clearly see from Fig. 5 that the obtained simulation results also closely match the analytical predictions.

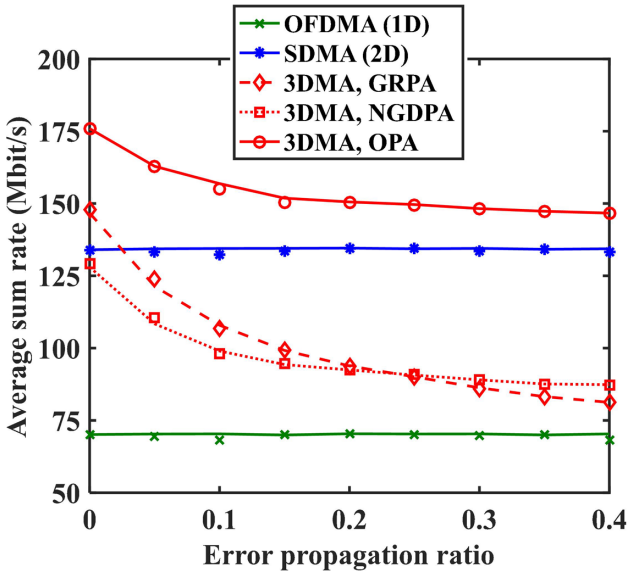

Fig. 6. Average sum rate versus error propagation ratio for hybrid 3DMA with GRPA, NGDPA, and OPA. Lines and markers show the analysis and simulation results, respectively.

We further study the impact of the error propagation level on the average sum rate of the 4×4 MIMO-VLC system applying different multiple access schemes, where the number of users is 15 and the transmitted SNR is 130 dB. Figure 6 shows the average sum rate versus the error propagation ratio for hybrid 3DMA with GRPA, NGDPA, and OPA, where the error propagation ratio β is assumed to be within the range of zero to 0.4. For the purpose of comparison, the average sum rates of OFDMA and SDMA are also plotted. It can be seen that the average sum rates of hybrid 3DMA with GRPA, NGDPA, and OPA all gradually decrease with the increase of the error propagation ratio β, which demonstrates the adverse effect of error propagation on the average sum rate of hybrid 3DMA due to imperfect SIC. Moreover, hybrid 3DMA with NGDPA always performs worse than SDMA, and hybrid 3DMA with GRPA obtains a higher sum rate than SDMA only when $\beta \leq 0.025$, suggesting that hybrid 3DMA with low-complexity channel-based PA strategies does not perform well under severe error propagation scenarios. However, we can see that hybrid 3DMA with OPA can always outperform SDMA even with an error propagation ratio as high as 0.4, which indicates that hybrid 3DMA with OPA exhibits better tolerance against the adverse error propagation effect. Similarly, it can also be found in Fig. 6 that the obtained simulation results and the analytical predictions have a good agreement, which verifies the validity of our derived analytical results.

Finally, we analyze the dynamic range of the achievable sum rate of the 4×4 MIMO-VLC system applying different multiple access schemes, where the transmitted SNR is 130 dB and the number of users is 15. Figures 7(a), 7(b), and 7(c) show the CDF plots of the sum rate for OFDMA, SDMA, and hybrid 3DMA with error propagation ratios of $\beta = 0$, 0.05, and 0.1, respectively. For the case of perfect SIC, i.e., $\beta = 0$, as shown in Fig. 7(a), the minimum sum rates achieved by OFDMA and SDMA are 40.1 and 66.7 Mbit/s, respectively. Moreover, the minimum sum rate obtained by hybrid 3DMA with OPA is 88.8 Mbit/s, indicating a 33.1% improvement of the minimum sum rate in comparison to SDMA. For the case of imperfect SIC with $\beta = 0.05$ and 0.1, as shown in Figs. 7(b) and 7(c), although the minimum sum rate of hybrid 3DMA with OPA is slightly reduced, it is still higher than that of SDMA. Therefore, hybrid 3DMA with OPA can achieve a much higher minimum sum rate than OFDMA and SDMA, which suggests that the proposed hybrid 3DMA with OPA exhibits excellent robustness and performance consistency to support multiple users with random locations over the receiving plane in the MU-MIMO-VLC system.

5. CONCLUSION

In this paper, we have proposed, analyzed, and evaluated a novel hybrid 3DMA scheme for MU-MIMO-VLC systems. All users within the system are first divided into multiple UGs, and the users within each UG are further divided into multiple UPs. For far and near users within each UP, power domain SPC is performed, and the corresponding OPA strategy is derived to maximize the achievable sum rate. Moreover, the impact of error propagation caused by imperfect SIC is also considered. The obtained simulation results successfully verify the validity of our analytical derivations. The analysis and simulation results show that the proposed hybrid 3DMA with OPA can substantially improve the achievable sum rate of the MU-MIMO-VLC system when compared with OFDMA and SDMA. More specifically, hybrid 3DMA with OPA achieves an average sum rate improvement of 32.8% in comparison to SDMA when the transmitted SNR is 130 dB, the number of users is 15, and the SIC is perfect. It is further revealed that

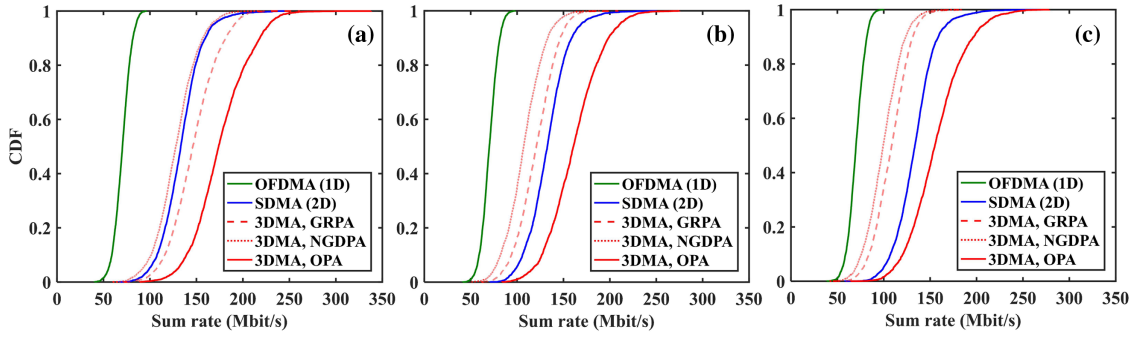

Fig. 7. CDF plot of the sum rate for OFDMA, SDMA, and hybrid 3DMA with error propagation ratios of (a) $\beta = 0$, (b) $\beta = 0.05$, and (c) $\beta = 0.1$.

hybrid 3DMA with OPA exhibits enhanced tolerance against error propagation and outperforms SDMA even with an error propagation ratio as high as 0.4. Moreover, hybrid 3DMA with OPA achieves a much higher minimum sum rate than OFDMA and SDMA, which shows excellent robustness and performance consistency to support multiple randomly located users in the MU-MIMO-VLC system. In conclusion, the proposed hybrid 3DMA scheme with OPA can be a promising candidate for MU-MIMO-VLC systems.

Finally, a few future directions can be suggested as follows: (1) theoretical and experimental evaluation of the proposed hybrid 3DMA scheme in practical MU-MIMO-VLC systems with low-pass frequency response and LED nonlinearity, (2) improved user pairing approaches by considering the distinctive quality-of-service requirement of each user, (3) analysis of user fairness in MU-MIMO-VLC systems applying the proposed hybrid 3DMA scheme.

Funding. National Natural Science Foundation of China (61901065); Natural Science Foundation of Chongqing (cstc2021jcyj-msxmX0480).

Disclosures. The authors declare no conflicts of interest.

REFERENCES

1. P. Yang, Y. Xiao, M. Xiao, and S. Li, "6G wireless communications: vision and potential techniques," IEEE Netw. **33**, 70–75 (2019).
2. T. Cogalan and H. Haas, "Why would 5G need optical wireless communications?" in *IEEE Annual International Symposium on Personal, Indoor and Mobile Radio Communications (PIMRC)* (2017).
3. C. Chen, D. A. Basnayaka, and H. Haas, "Downlink performance of optical attocell networks," J. Lightwave Technol. **34**, 137–156 (2016).
4. H. Haas, "Visible light communication," in *Optical Fiber Communication Conference (OFC)* (2015), paper Tu2G.5.
5. N. Chi, Y. Zhou, Y. Wei, and F. Hu, "Visible light communication in 6G: advances, challenges, and prospects," IEEE Veh. Technol. Mag. **15**(4), 93–102 (2020).
6. T. Komine and M. Nakagawa, "Fundamental analysis for visible-light communication system using LED lights," IEEE Trans. Consum. Electron. **50**, 100–107 (2004).
7. Y. Yang, J. Luo, C. Chen, and L. Chen, "Enabling real-life deployment of piggyback-VLC via light emission composition," IEEE Internet Comput. **24**, 59–65 (2020).
8. J.-Y. Sung, C.-W. Chow, and C.-H. Yeh, "Is blue optical filter necessary in high speed phosphor-based white light LED visible light communications?" Opt. Express **22**, 20646–20651 (2014).
9. X. Huang, Z. Wang, J. Shi, Y. Wang, and N. Chi, "1.6 Gbit/s phosphorescent white LED based VLC transmission using a cascaded pre-equalization circuit and a differential outputs PIN receiver," Opt. Express **23**, 22034–22042 (2015).
10. C. Chen, Y. Nie, M. Liu, Y. Du, R. Liu, Z. Wei, H. Fu, and B. Zhu, "Digital pre-equalization for OFDM-based VLC systems: centralized or distributed?" IEEE Photon. Technol. Lett. **33**, 1081–1084 (2021).
11. H. Le Minh, D. O'Brien, G. Faulkner, L. Zeng, K. Lee, D. Jung, Y. Oh, and E. T. Won, "100-Mb/s NRZ visible light communications using a postequalized white LED," IEEE Photon. Technol. Lett. **21**, 1063–1065 (2009).
12. H. Li, X. Chen, B. Huang, D. Tang, and H. Chen, "High bandwidth visible light communications based on a post-equalization circuit," IEEE Photon. Technol. Lett. **26**, 119–122 (2014).
13. L. Zeng, D. C. O'Brien, H. Le Minh, G. E. Faulkner, K. Lee, D. Jung, Y. Oh, and E. T. Won, "High data rate multiple input multiple output (MIMO) optical wireless communications using white LED lighting," IEEE J. Sel. Areas Commun. **27**, 1654–1662 (2009).
14. G. Stepniak, M. Schüppert, and C.-A. Bunge, "Advanced modulation formats in phosphorous LED VLC links and the impact of blue filtering," J. Lightwave Technol. **33**, 4413–4423 (2015).
15. M. Obeed, A. M. Salhab, M.-S. Alouini, and S. A. Zummo, "On optimizing VLC networks for downlink multi-user transmission: a survey," IEEE Commun. Surv. Tutorials **21**, 2947–2976 (2019).
16. C. Chen, H. Yang, P. Du, W.-D. Zhong, A. Alphones, Y. Yang, and X. Deng, "User-centric MIMO techniques for indoor visible light communication systems," IEEE Syst. J. **14**, 3202–3213 (2020).
17. T. Fath and H. Haas, "Performance comparison of MIMO techniques for optical wireless communications in indoor environments," IEEE Trans. Commun. **61**, 733–742 (2013).
18. P. F. Mmbaga, J. Thompson, and H. Haas, "Performance analysis of indoor diffuse VLC MIMO channels using angular diversity detectors," J. Lightwave Technol. **34**, 1254–1266 (2016).
19. C. Chen, W.-D. Zhong, and D. Wu, "On the coverage of multiple-input multiple-output visible light communications [Invited]," J. Opt. Commun. Netw. **9**, D31–D41 (2017).
20. N. Huang, X. Wang, and M. Chen, "Transceiver design for MIMO VLC systems with integer-forcing receivers," IEEE J. Sel. Areas Commun. **36**, 66–77 (2018).
21. H. Yang, C. Chen, W.-D. Zhong, and A. Alphones, "Joint precoder and equalizer design for multi-user multi-cell MIMO VLC systems," IEEE Trans. Veh. Technol. **67**, 11354–11364 (2018).
22. S. Rajbhandari, H. Chun, G. Faulkner, H. Haas, E. Xie, J. J. McKendry, J. Herrnsdorf, E. Gu, M. D. Dawson, and D. O'Brien, "Neural network-based joint spatial and temporal equalization for MIMO-VLC system," IEEE Photon. Technol. Lett. **31**, 821–824 (2019).
23. A. H. Azhar, T.-A. Tran, and D. O'Brien, "A gigabit/s indoor wireless transmission using MIMO-OFDM visible-light communications," IEEE Photon. Technol. Lett. **25**, 171–174 (2013).
24. A. Burton, H. Le Minh, Z. Ghassemlooy, E. Bentley, and C. Botella, "Experimental demonstration of 50-Mb/s visible light communications using 4×4 MIMO," IEEE Photon. Technol. Lett. **26**, 945–948 (2014).
25. H. G. Olanrewaju, J. Thompson, and W. O. Popoola, "Pairwise coding for MIMO-OFDM visible light communication," IEEE Trans. Wireless Commun. **19**, 1210–1220 (2019).
26. S. M. Mana, P. Hellwig, J. Hilt, K. L. Bober, V. J. Hirmanova, P. Chvojka, R. Janca, and S. Zvanovec, "LiFi experiments in a hospital," in *Optical Fiber Communication Conference (OFC)* (2020), paper M3I.2.
27. S. M. Mana, V. Jungnickel, K. L. Bober, P. Hellwig, J. Hilt, D. Schulz, A. Paraskevopoulos, R. Freund, K. Hirmanova, R. Janca, P. Chvojka, and S. Zvanovec, "Distributed multiuser MIMO for LiFi: experiments in an operating room," J. Lightwave Technol. **39**, 5730–5743 (2021).
28. M. Biagi, A. M. Vegni, and T. D. Little, "LAT indoor MIMO-VLC—localize, access and transmit," in *International Workshop on Optical Wireless Communications (IWOW)* (2012).
29. J. Lian and M. Brandt-Pearce, "MIMO signal processing for multiuser VLC systems," in *IEEE Photonics Society Summer Topical Meeting Series (SUM)* (2016), pp. 60–61.
30. J. Lian and M. Brandt-Pearce, "Multiuser MIMO indoor visible light communication system using spatial multiplexing," J. Lightwave Technol. **35**, 5024–5033 (2017).
31. J. Lian, Y. Gao, P. Wu, G. Zhu, and Y. Wang, "Indoor MIMO VLC systems using optical orthogonal frequency division multiple access," Opt. Commun. **485**, 126728 (2021).
32. B. Lin, Z. Ghassemlooy, X. Tang, Y. Li, and M. Zhang, "Experimental demonstration of optical MIMO NOMA-VLC with single carrier transmission," Opt. Commun. **402**, 52–55 (2017).
33. C. Chen, W.-D. Zhong, H. Yang, and P. Du, "On the performance of MIMO-NOMA-based visible light communication systems," IEEE Photon. Technol. Lett. **30**, 307–310 (2018).
34. H. Wang, F. Wang, and R. Li, "Enhancing power allocation efficiency of NOMA aided-MIMO downlink VLC networks," Opt. Commun. **454**, 124497 (2020).
35. Y. Hong, J. Chen, Z. Wang, and C. Yu, "Performance of a precoding MIMO system for decentralized multiuser indoor visible light communications," IEEE Photon. J. **5**, 7800211 (2013).
36. Y. Fan, Q. Zhao, B. Kang, and L. Deng, "Equivalent ZF precoding scheme for downlink indoor MU-MIMO VLC systems," Opt. Commun. **407**, 402–409 (2018).

37. C. Chen, Y. Yang, X. Deng, P. Du, and H. Yang, "Space division multiple access with distributed user grouping for multi-user MIMO-VLC systems," IEEE Open J. Commun. Soc. **1**, 943–956 (2020).
38. A. M. Abdelhady, O. Amin, A. Chaaban, B. Shihada, and M.-S. Alouini, "Downlink resource allocation for dynamic TDMA-based VLC systems," IEEE Trans. Wireless Commun. **18**, 108–120 (2019).
39. Y. Qiu, S. Chen, H.-H. Chen, and W. Meng, "Visible light communications based on CDMA technology," IEEE Wireless Commun. **25**, 178–185 (2018).
40. J.-Y. Sung, C.-H. Yeh, C.-W. Chow, W.-F. Lin, and Y. Liu, "Orthogonal frequency-division multiplexing access (OFDMA) based wireless visible light communication (VLC) system," Opt. Commun. **355**, 261–268 (2015).
41. H. Marshoud, V. M. Kapinas, G. K. Karagiannidis, and S. Muhaidat, "Non-orthogonal multiple access for visible light communications," IEEE Photon. Technol. Lett. **28**, 51–54 (2016).
42. C. Chen, S. Fu, X. Jian, M. Liu, X. Deng, and Z. Ding, "NOMA for energy-efficient LiFi-enabled bidirectional IoT communication," IEEE Trans. Commun. **69**, 1693–1706 (2021).
43. H. Sadat, M. Abaza, A. Mansour, and A. Alfalou, "A survey of NOMA for VLC systems: research challenges and future trends," Sensors **22**, 1395 (2022).
44. K. Ying, Z. Yu, R. J. Baxley, H. Qian, G.-K. Chang, and G. T. Zhou, "Nonlinear distortion mitigation in visible light communications," IEEE Wireless Commun. **22**, 36–45 (2015).
45. P. Chvojka, S. Zvanovec, P. Haigh, and Z. Ghassemlooy, "Channel characteristics of visible light communications within dynamic indoor environment," J. Lightwave Technol. **33**, 1719–1725 (2015).
46. C. Chen, X. Zhong, S. Fu, X. Jian, M. Liu, H. Yang, A. Alphones, and H. Y. Fu, "OFDM-based generalized optical MIMO," J. Lightwave Technol. **39**, 6063–6075 (2021).
47. Z. Ding, X. Lei, G. K. Karagiannidis, R. Schober, J. Yuan, and V. K. Bhargava, "A survey on non-orthogonal multiple access for 5G networks: research challenges and future trends," IEEE J. Sel. Areas Commun. **35**, 2181–2195 (2017).
48. H. Li, Z. Huang, Y. Xiao, S. Zhan, and Y. Ji, "Solution for error propagation in a NOMA-based VLC network: symmetric superposition coding," Opt. Express **25**, 29856–29863 (2017).
49. C. Chen, W.-D. Zhong, H. Yang, P. Du, and Y. Yang, "Flexible-rate SIC-free NOMA for downlink VLC based on constellation partitioning coding," IEEE Wireless Commun. Lett. **8**, 568–571 (2019).
50. T. Lipp and S. Boyd, "Variations and extension of the convex–concave procedure," Optim. Eng. **17**, 263–287 (2016).
51. Hamamatsu Photonics, "Si APDs," s8664 series datasheet (2020).